ECS Journal of Solid State
Science and Technology

OPEN ACCESS

Effect of Dry Etching to Improve Ohmic Contacts on Bulk, Lightly-Doped β-Ga_2O_3

To cite this article: Chao-Ching Chiang *et al* 2024 *ECS J. Solid State Sci. Technol.* **13** 015001

View the article online for updates and enhancements.

You may also like

- The Role of Alanine in the Chemical Mechanical Polishing of Aluminum
Yuwei Cao, Shengli Wang, Chong Luo et al.

- Spectroscopic and Judd-Ofelt Analysis of Nd^{3+} Ion Doped Lithium Antimony-Borate Glasses for Visible and Near Infrared Laser Application Compared to Standard Emission at 1.06 m
M. Iezid, A. Abidi, F. Goumeidane et al.

- Numerical Simulation of Hetero Dielectric Trench Gate JAM Gate-All-Around FET (HDTG-JAM-GAAFET) for Label Free Biosensing Applications
Shivani Yadav and Sonam Rewari

Measure the Electrode Expansion in the Nanometer Range.
Discover the new ECD-4-nano!
EL-CELL®
electrochemical test equipment

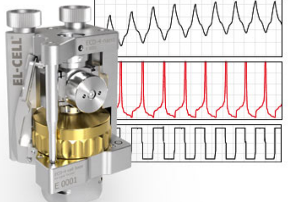

• Battery Test Cell for Dilatometric Analysis (Expansion of Electrodes)
• Capacitive Displacement Sensor (Range 250 µm, Resolution ≤ 5 nm)
• Detect Thickness Changes of the Individual Electrode or the Full Cell.

www.el-cell.com +49 40 79012-734 sales@el-cell.com

This content was downloaded from IP address 128.227.126.34 on 07/04/2024 at 11:47

ECS Journal of Solid State Science and Technology, 2024 **13** 015001

Effect of Dry Etching to Improve Ohmic Contacts on Bulk, Lightly-Doped β-Ga_2O_3

Chao-Ching Chiang,[1,z] Jian-Sian Li,[1] Hsiao-Hsuan Wan,[1] Fan Ren,[1,*] and Stephen J. Pearton[2,*]

[1]*Department of Chemical Engineering, University of Florida, Gainesville, Florida 32611, United States of America*
[2]*Department of Material Science and Engineering, University of Florida, Gainesville, Florida 32611, United States of America*

Ti/Au is a typical Ohmic metal contact stack to n-type β-Ga_2O_3 but there have been few systematic studies of the use of pre-exposure of the surface to plasmas prior to metal deposition in order to lower the contact resistance. The effects of Cl_2/Ar Inductively Coupled Plasma exposure of Ga_2O_3 surfaces prior to deposition of Ti/Au (20/80 nm) contacts were examined through circular transfer length method (CTLM) measurements to determine both the contact resistance and specific contact resistivity. ICP source power, which controls ion density in the plasma is found to be more important than ion energy (~165–490 eV in these experiments). The plasma exposure improved specific contact resistivity by more than a factor of 2 in all cases for lightly n-type (10^{17} cm^{-3}) Ga_2O_3 and a minimum value of 2×10^{-4} Ω.cm^2 was obtained after heating at 550 °C.
© 2024 The Author(s). Published on behalf of The Electrochemical Society by IOP Publishing Limited. This is an open access article distributed under the terms of the Creative Commons Attribution 4.0 License (CC BY, http://creativecommons.org/licenses/by/4.0/), which permits unrestricted reuse of the work in any medium, provided the original work is properly cited. [DOI: 10.1149/2162-8777/ad1618]

Manuscript submitted October 4, 2023; revised manuscript received November 10, 2023. Published January 10, 2024.

The β-polytype of Ga_2O_3, with its ultra-wide bandgap (4.5–4.9 eV), high breakdown voltage, and reasonable electron transport properties, has gained attention as a candidate for next-generation power electronics. The wide bandgap of Ga_2O_3 allows for higher breakdown voltage, reducing leakage current and enabling high-power operation. The efficiency of switching is also higher at a given voltage than materials like GaN or SiC. There has been much progress in Ga_2O_3 power device development over the past decade. Ga_2O_3-based Schottky diodes exhibit low reverse leakage current and high breakdown voltages, making them ideal for rectification and power conversion, enabling efficient conversion and distribution of energy from sources like solar and wind. Ga_2O_3 power electronics can also enhance the performance of electric vehicle (EV) drive-trains and charging systems. Their high-power capability and energy efficiency contribute to extended EV range and faster charging.

Despite its potential, Ga_2O_3 power electronics faces challenges, including improving the quality of Ga_2O_3 substrates to reduce defects and enhance device performance, developing suitable gate dielectrics for Ga_2O_3 transistors with low gate leakage and high reliability, and expanding the commercial production of Ga_2O_3 substrates and devices to make them cost-effective for widespread adoption.

In Ga_2O_3 device fabrication, low-resistance Ohmic contacts are crucial.[1–12] High contact resistance degrades device switching speeds and exacerbates reliability concerns due to the localized heating generated at the contact interface during current flow in device operation.[2–7]

Low-resistance Ohmic contacts in Ga_2O_3 power electronics minimize power dissipation,[1–3] while high-resistance contacts result in increased Joule heating. The increased temperature can degrade device reliability and efficiency.[3,4] Low resistance Ohmic contacts mitigate this issue by minimizing power losses, ensuring higher overall device efficiency, and facilitating higher current-carrying capacity in Ga_2O_3 power devices.[13,14] Low-resistance Ohmic contacts also play a pivotal role in voltage compatibility.[15–18] Ga_2O_3 power devices are designed for high-voltage applications, and high-resistance contacts can lead to excessive voltage drop and breakdown at the contact-semiconductor interface. Low resistance contacts alleviate this issue, ensuring that the device can operate at its specified voltage rating without voltage-related failures.

A specific example of the need for low resistance contacts are the backside contacts for vertical rectifier structures. In this case, plasma exposure and other methods have been used to create higher n-type doping levels in the near-surface region, which promotes lower contact resistance. Such treatment of the surface during fabrication is a common step on producing Ohmic contacts to wide bandgap semiconductors. Strategies employed for the formation of such junctions primarily involve the reduction of the Schottky barrier height at the contact interface. Traditional strategies for lowering contact resistance include increasing the carrier concentration beneath the contact through ion implantation,[9,13–15] creation of vacancy-related donor entities, or alternatively, the incorporation of a low-resistance interlayer.[19–23] Another method to improve contact resistance is post-deposition annealing of the contact metallization to create an interlayer, which reduces the discontinuity of the conduction band between the semiconductor and metal.[24–26] Surface defects introduced during RIE etching and ion bombardment in β- Ga_2O_3 can subsequently serve as centers for carrier recombination post-metallization, thereby diminishing contact resistance.

Typical Ohmic contacts on Ga_2O_3 employ a multilayer metal contact stack comprising at least one low work function metal and one or more high work function metals.[2,3,27,28] Surface treatment prior to metallization plays a pivotal role in the barrier height and device stability. Yao et al.[6] showed the impact of distinct wet chemical treatments on unpassivated surface states and bulk or near-surface states held greater sway in dictating the electrical behavior of rectifying contacts compared to the choice of metals.

To facilitate electron tunneling across the junction, Si-ion implantation was used to create a heavily doped n^+-region.[13] However, this process necessitates elevated temperature annealing (>900 °C) for the activation of Si donors. Plasma bombardment and Reactive Ion Etching (RIE) have also been explored as alternative pretreatment techniques prior to metallization. Higashiwaki et al.[15] demonstrated that the Schottky-like Ti/Au contacts converted to Ohmic-like contacts after RIE, a transformation linked to the generation of oxygen vacancies. Wang et al.[11] reported that Ar plasma bombardment for 30 s reduced contact resistance by increasing surface n-type doping. The combined application of RIE and Si ion implantation yielded a specific contact resistance of 8.1×10^{-6} Ω cm^2, underscoring the potential for enhancing Ohmic contact properties through the synergistic utilization of these techniques.[1–11]

A typical metallization for n-type Ga_2O_3 Ohmic contacts is Ti/Au. Ti is chosen for its low work function and robust adhesion to Ga_2O_3, while Au possesses low resistivity and functions as a current

*Electrochemical Society Fellow.
zE-mail: cchiang@ufl.edu

Table I. Summary of etch conditions, including the plasma powers, etch depth, and dc self-bias on the electrode.

RF power	(W)	100	250	400	100	250	400
ICP power	(W)	200	200	200	600	600	600
Etch depth	(nm)	30	60	90	80	110	140
DC bias	(V)	233	466	633	142	300	400

spreading layer.[3–7] On very heavily doped n-Ga_2O_3, specific contact resistivities in the range of 10^{-5}–10^{-6} Ω·cm^2 have been reported[1,2] but the bigger challenge is to make low resistance Ohmic contacts on lightly doped n-Ga_2O_3 of the type encountered in transistor channels or rectifier drift regions, i.e. at the 10^{17} cm^{-3} doping level. It is in these applications that techniques for lowering contact resistance are needed and is the subject of this work. For the low doping levels, typical specific contact resistivities are $>10^{-2}$ Ω.cm^2 without employing surface modification techniques.

Despite the widespread adoption of plasma etching for β-Ga_2O_3 surfaces in Ohmic contact applications, little attention has been devoted to quantifying the interplay between the plasma parameters and their influence on the specific contact resistivity.[2] In the present study, we demonstrate their influence on the contact resistivity of the Ti/Au Ohmic contact and the prevailing transport mechanisms.

Experimental

Nominally undoped (201) Ga_2O_3 substrates with n-type doping $\sim10^{17}$ cm^{-3} were used for these experiments (Novel Crystal Technologies). The circular transfer length method (CTLM) was employed to measure both contact resistance and specific contact resistivity. These patterns were fabricated by the use of standard photolithography, combined with electron beam metal evaporation in a 4-pocket Oxford Instruments system with a base pressure $<10^{-7}$ Torr, and subsequent liftoff of Ti/Au (20/80 nm). The circular TLM design had an outer ring radius R = 120 μm and an inner ring radius r = 115/110/105/95/85/75 μm. After depositing the metal contact range of circular TLM patterns with increasing gap widths are fabricated, Prior to metal deposition, the samples were exposed to Inductively Coupled Plasmas (ICP) under different conditions. The etching was performed in a PlasmaTherm 790 Inductively Coupled Plasma reactor with Cl_2/Ar discharges (respective flow rates 15/5 sccm) and 5 mTorr process pressure.[29,30] The RF power on the lower electrode was either 100, 250, or 400 W, while the ICP power was 200 or 600 W. The etch depths and DC self-bias on the powered electrode are summarized in Table I.

After the plasma exposure, the contacts were deposited and annealed (all in N_2) at 400 °C 1 min, 450 °C 1 min, 475 °C 1 min, 500 °C 1 min, 525 °C 1 min or 550 °C from 1 to 5 min. Examples of the CLTM patterns before and after the anneal are shown in Fig. 1, with (a) a schematic of the contact structures measured, along with optical images of 15 μm gap (R/r = 120/105 μm) circular TLM patterns, both (b) as-deposited and (c) after 550 °C, 5 min N_2 RTA. The current-voltage characteristics for different spacings were used to determine the transfer resistance, sheet resistance, and contact resistance as a function of process conditions. The current density-voltage (J–V) characteristics, were obtained using a Tektronix 370-A curve tracer, 371-B curve, and Agilent 4156C.

We also measured the temperature dependence of these parameters in order to determine the dominant current transport under different conditions, expected to be either thermionic or field emission at our doping levels. According to the thermionic emission (TE) and field emission (FE) models, the equations for specific contact resistivities are:

$$\text{Field emission: } \rho_c \propto \exp(\Phi_b/E_{00}), \text{ where } E_{00} = eh/4\pi\,[N_D/m^*\varepsilon_s]^{1/2},$$

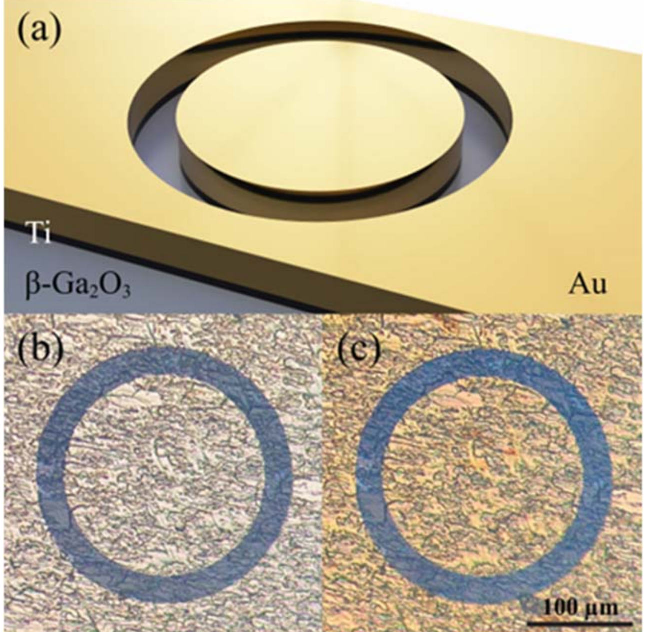

Figure 1. (a) Schematic and optical images of 15 μm gap (R/r = 120/105 μm) circular TLM pattern (b) as deposited (c) after 550 °C 5 min N_2 RTA.

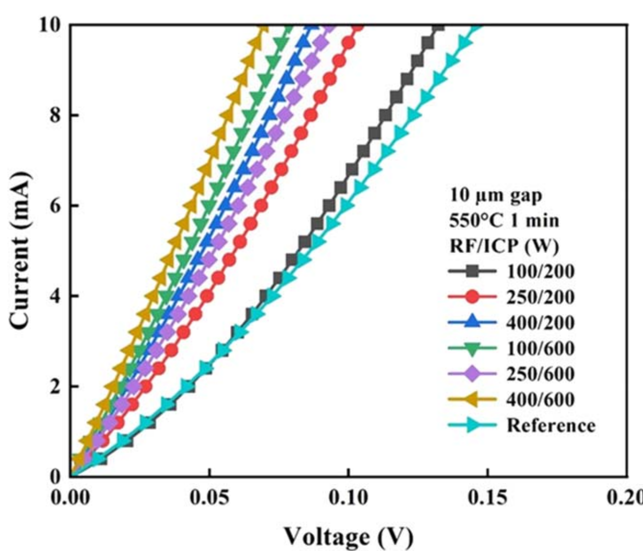

Figure 2. I-V curves of 10 μm gap circular TLM with different etching conditions after 550 °C 1-min N_2 RTA. The reference sample was an unetched control.

and

$$\text{Thermionic emission: } \rho_c \propto \exp(q\Phi_b/kT).$$

In these equations, ρ_c is specific contact resistivity, ϕ_b is barrier height, e electronic charge, h is Panck's constant, N_D is the doping in the Ga_2O_3, m^* the electron effective mass and ε_s the semiconductor permittivity.

The value of the characteristic energy E_{00} is around 3×10^{-3} eV at room temperature for the doping in our samples. E_{00} is inversely proportional to electron tunneling probability through the metal-semiconductor contact. If there is little temperature dependence of the contact resistance, it would suggest that FE is the dominant mechanism.[31,32]

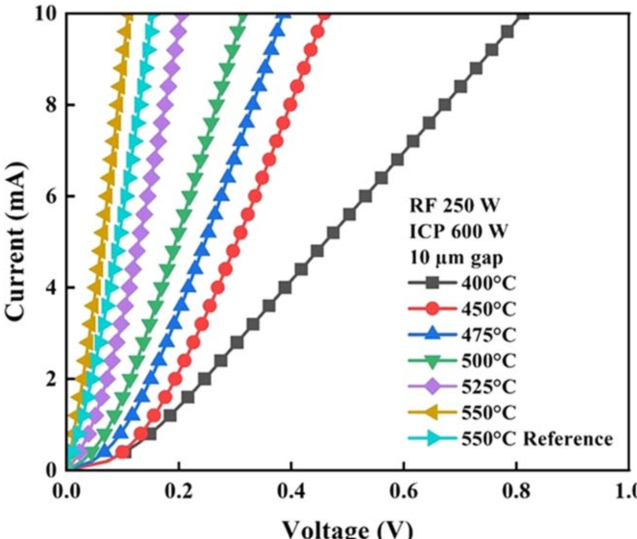

Figure 3. I-V curves of 10 μm gap circular TLM with different annealing temperatures on the sample with an etching condition of RF 250 W/ ICP 600 W. The reference sample was an unetched control.

Results

Figure 2 shows I-V curves of 10 μm gap circular TLM with different etching conditions after 550 °C, 1 min N_2 RTA. Note that the current increases for all the etch conditions, relative to the unetched control samples annealed at the same conditions. The highest currents are obtained for the highest ICP source power of 600 W, which shows that plasma density is important as well as the incident ion energy. The latter is determined by the rf power on the sample position. The majority ions present are Ar^+, with a minority of Cl_2 positive and negative ions, as determined from mass spectrometry measurements on this reactor. The combination of the initial ion energy and the acceleration provided by the DC self-bias developed on the powered electrode means the resultant average ion energy is the addition of this DC self-bias, plus the plasma sheath potential. This sheath potential is $\sim$23 V under the conditions used in the experiments. Therefore, the ion energies range from $\sim$165–490 eV over the range of conditions we examined. When both plasma powers were low (100/200 W), the improvement in current was the lowest, being fairly similar to the unetched control samples. This is despite the fact the average ion energy is $\sim$256 eV, which will cause disruption of the Ga_2O_3 surface, but since the ICP source power and hence ion flux is low, there is less enhancement of the current through the contact.

At a fixed set of plasma powers, the effect of annealing temperature was investigated. Figure 3 shows I-V curves of 10 μm gap circular TLM with different annealing temperatures on the sample with a fixed etching condition of RF 250 W/ ICP 600 W. Note that the current at fixed voltage increases as the annealing temperature increases. The samples annealed at 550 °C show an improvement due to the plasma exposure compared to the reference sample that was only annealed. It is important to remember that temperature is the dominant effect over time in these experiments since the contact reactions are exponentially dependent on temperature but only on the square root of time.

Figure 4 shows the calculated transfer resistance, sheet resistance, and specific contact resistivity with different etching conditions and annealing temperatures. Note that plasma power conditions as well as subsequent annealing temperature have significant effects on all three of these parameters, meaning it is possible to get relatively low specific contact resistivities even for annealing temperatures as low as 400 °C. The large variations in R_C at annealing temperatures <500 °C show how important it is to optimize the plasma exposure conditions in order to get the lowest

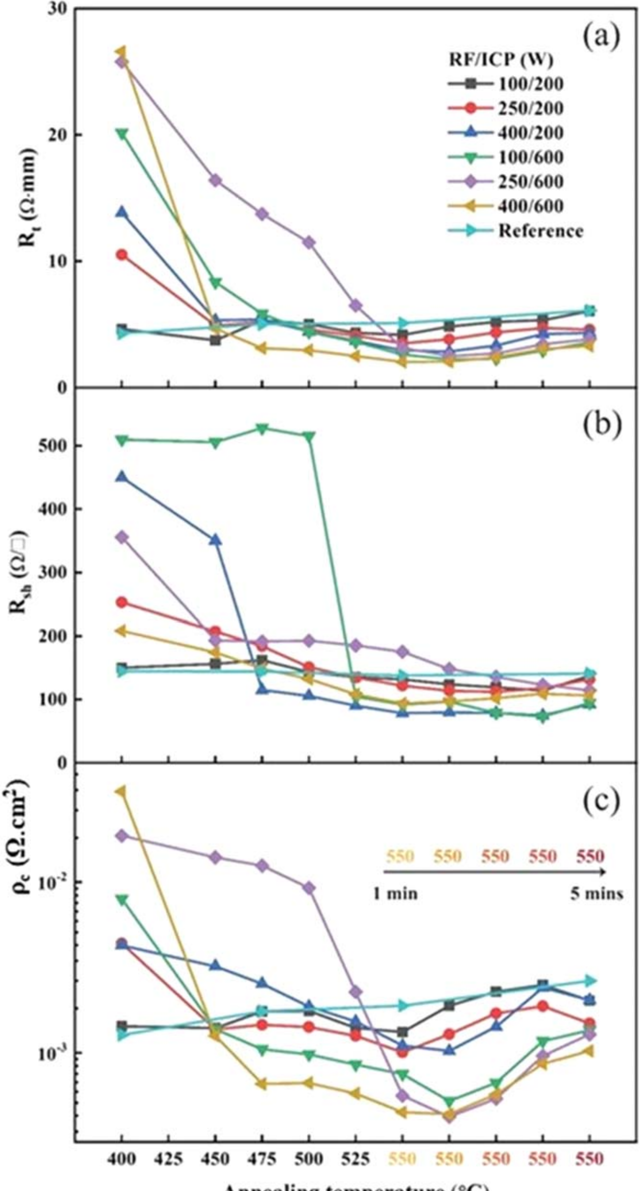

Figure 4. Calculated (a) transfer resistance, (b) sheet resistance, and (c) specific contact resistivity with different etching conditions and annealing temperatures. The reference samples were unetched controls.

contact resistance. The sheet resistance is a significant contributor to the final value of R_c. The minimum value of ρ_c obtained was $2 \times 10^{-4}\ \Omega.cm^2$, which is lower by 30%–50% than the best values reported for the n-type doping level used here, in which plasma exposure was used to lower the original specific contact resistivity.[1,2] We note that we measured three different contact structures for each condition and took the average to get the data points in Fig. 4. Note that the 100/600 W condition is one where the ion energy is lowest, but the plasma density is highest, so that may produce a situation where chemical effects begin to compete with the ion damage effects.

Figure 5 shows the calculated temperature-dependent specific contact resistivity using an etching condition of RF 400 W/ICP 600 W. At room temperature, the plasma-treated contacts have specific contact resistivities approximately 2.5 times lower than the reference devices. Both have significant dependencies on temperatures below 150 °C but are relatively insensitive at higher temperatures. This is consistent with a transition from thermionic emission to field

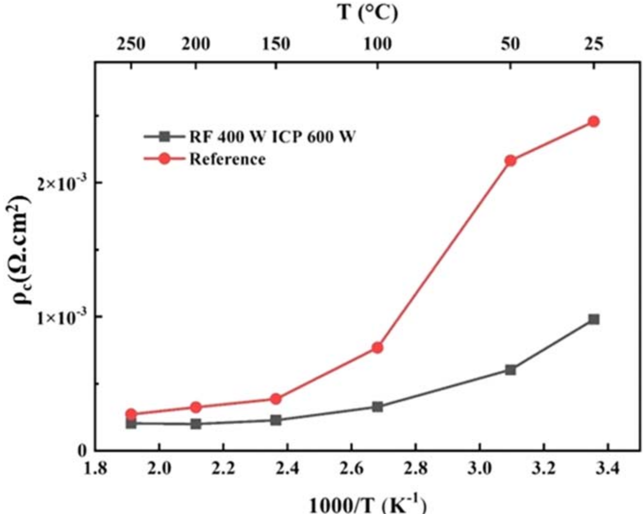

Figure 5. Calculated temperature-dependent specific contact resistivity using circular TLM on the etched surface with an etching condition of RF 400 W/ ICP 600 W. The reference sample was an unetched control.

emission, where electrons tunnel through the barrier at this temperature. The transition likely involves thermionic field emission, in which some electrons are promoted over the potential barrier, while others tunnel through the barrier. The barrier height for Ti on the as-received surfaces is ~1.1 eV, but after plasma damage is reduced to 0.8 eV, consistent with the increased tunneling probability and improved contact resistance. These were obtained by fitting the forward I-V in the normal manner assuming thermionic emission.[1,2] We also note that the RF and ICP powers are inter-related, but allow control of both ion energy and density. Thus the study here has more flexibility in controlling these parameters than studies where only an RIE system is used, in which an increase in ion energy must always be accompanied by an increase in ion density.

Discussion

To achieve low contact resistance with Ohmic contacts to ultra-wide bandgap semiconductors like Ga_2O_3 is generally difficult. This can be more difficult in β-Ga_2O_3 due to the presence of upward surface band bending[2] and, thus, many mentalizations are usually rectifying. Ti-based contact stacks with Ti as the contact metal touching the Ga_2O_3 surface are the most prevalent, i.e. Ti/Au or Ti/Al/Ni/Au. Results in the literature on β-Ga_2O_3 show the magnitude of the metal work function does not correlate with the ability to form Ohmic contacts and use of localized doping plasma exposure have been successfully used to enhance Ohmic contact formation.

In this work, we observed that short exposures of the surface of Ga_2O_3 to Cl_2/Ar discharges led to improved specific contact resistivities, with the amount of improvement being a function of both plasma density and average ion energy. We quantified the relationship between the plasma processing conditions and the influence of surface damage on specific contact resistivity. The etching during the plasma process will change the surface band-bending normally present due to adsorbed hydroxyl species. Swallow et al.[33] reported that uncleaned (_201) β-Ga_2O_3 surfaces showed hydroxyl groups which produce a downward band-bending of −0.24 eV due to the presence of an electron accumulation layer. These hydroxyl species could be removed by annealing at 800 °C, which dramatically changed the band bending to an upward value of 0.26 eV. This cleaned surface exhibited electron depletion after desorption of the native hydroxyl groups. Additional work on hydroxide adsorption and desorption on (_201) β-Ga_2O_3 surfaces with surface treatments by Gazoni et al.[12] showed that as-received samples were terminated with OH^- groups, but these could be removed by 15-min anneal at 600 °C under vacuum conditions. The removal of OH^- produced a transition to upward band bending from ~0.5 to 1.0 eV, consistent with the work of Swallow et al.[33]

In our case, the etching step removes the hydroxyl layer and creates a damaged region approximately 100 nm deep,[34] which is further than the range of the ions in the discharges and caused by fast diffusion of point defects into the bulk during the etching. The most likely point defects created are Ga vacancies, (V_{Ga}) which have high diffusivities in Ga_2O_3 since the migration barriers for diffusion are smaller than the barriers for oxygen vacancies, on average by at least 1 eV.[35] These defects reduce the carrier concentration in the damaged region, which would increase contact resistance, but this is offset by the reduced barrier and increased chance for tunneling through defect states. This explains why there is a complex relation between the magnitude of the contact improvement and the interplay between the two plasma powers since the resultant etch rate also determines the depth at which compensating vacancy defects will be present.

This work shows a pathway to lowering the Ohmic contact resistance on lightly doped n-Ga_2O_3 of the type typically used in transistor channels and rectifier drift regions. Our process uses a simple plasma exposure under optimized conditions, where ion-induced damage creates a pathway for additional current conduction. The specific contact resistivities achieved are lower by more than a factor of 2 compared to previous reports on n-Ga_2O_3 of this doping level that were exposed to plasmas to lower the specific contact resistivity.[1,2]

It will be interesting to see if similar trends are obtained with different orientations of Ga_2O_3. For example, it has been previously noted that the Ti/(001) Ga_2O_3 surface oxidizes more than the Ti/(010) Ga_2O_3 surface.[36] This demonstrates the strong difference in reactivity of the same material with different surface orientations.

Conclusions

In this study, we investigated the effects of Cl_2/Ar Inductively Coupled Plasma (ICP) exposure on β-Ga_2O_3 surfaces prior to the deposition of Ti/Au Ohmic contacts. We employed the circular transfer length method (CTLM) measurements to assess contact resistance and specific contact resistivity. Our experiments demonstrated that Cl_2/Ar ICP exposure significantly improved specific contact resistivity by more than a factor of 2 in all cases. Notably, the ICP source power, which controls ion density in the plasma, was found to be more critical than ion energy. Annealing temperature was also investigated, and it was observed that higher annealing temperatures led to improved current characteristics. Plasma-exposed contacts showed better performance compared to unexposed contacts at the same annealing temperature. The temperature-dependent contact resistance analysis revealed that plasma-treated contacts exhibited specific contact resistivities approximately 2.5 times lower than reference devices at room temperature. The transition from thermionic emission to field emission was observed at temperatures around 150 °C. Plasma etching created a damaged layer on the Ga_2O_3 surface, removing hydroxyl groups and introducing vacancy defects. While this damaged layer could theoretically increase contact resistance, it was offset by the reduced barrier and increased chance for tunneling through defect states.

In conclusion, our systematic study demonstrates the significant impact of Cl_2/Ar ICP exposure on lowering the specific contact resistivity of Ti/Au Ohmic contacts to n-type β-Ga_2O_3. The interplay between plasma parameters, annealing temperature, and surface damage played a crucial role in achieving low-resistance Ohmic contacts. We were able to lower the specific contact resistivity by more than a factor of 2 relative to previous studies where only RIE systems were used. This research contributes to optimizing contact properties for Ga_2O_3 power devices.

Acknowledgments

This research at UF was performed as part of the Interaction of Ionizing Radiation with Matter University Research Alliance (IIRM-URA), sponsored by the Department of the Defense, Defense Threat Reduction Agency under the award HDTRA1–20–2–0002. The

content of the information does not necessarily reflect the position or the policy of the federal government, and no official endorsement should be inferred. This work at UF was also supported by NSF DMR 1856662.

ORCID

Chao-Ching Chiang https://orcid.org/0000-0002-0447-8170
Jian-Sian Li https://orcid.org/0000-0002-2817-7612
Hsiao-Hsuan Wan https://orcid.org/0000-0002-6986-8217
Stephen J. Pearton https://orcid.org/0000-0001-6498-1256

References

1. H. Sheoran, V. Kumar, and R. Singh, *ACS Applied Electronic Materials*, **4**, 2589 (2022).
2. L. A. Lyle, *J. Vac. Sci. Technol. A*, **40**, 060802 (2022).
3. H. Kim, *SN Applied Sciences*, **4**, 27 (2022).
4. Y.-W. Huan, S.-M. Sun, C.-J. Gu, W.-J. Liu, S.-J. Ding, H.-Y. Yu, C.-T. Xia, and D. W. Zhang, *Nanoscale Res. Lett.*, **13**, 1 (2018).
5. C. Lu, X. Ji, Z. Liu, X. Yan, N. Lu, P. Li, and W. Tang, *J. Phys. D: Appl. Phys.*, **55**, 463002 (2022).
6. Y. Yao, R. F. Davis, and L. M. Porter, *J. Electron. Mater.*, **46**, 2053 (2017).
7. L. A. Lyle, T. C. Back, C. T. Bowers, A. J. Green, K. D. Chabak, D. L. Dorsey, E. R. Heller, and L. M. Porter, *APL Mater.*, **9**, 061104 (2021).
8. M.-H. Lee, T.-S. Chou, S. Bin Anooz, Z. Galazka, A. Popp, and R. L. Peterson, *ACS nano*, **16**, 11988 (2022).
9. L. A. Lyle, S. Okur, V. S. Chava, M. L. Kelley, R. F. Davis, G. S. Tompa, M. Chandrashekhar, A. B. Greytak, and L. M. Porter, *J. Electron. Mater.*, **49**, 3490 (2020).
10. B. Kim, H. Park, S. Lee, D. Lee, C. Jung, and H. Jeon, *ECS J. Solid State Sci. Technol.*, **11**, 053009 (2022).
11. C. Wang, J. Zhang, S. Xu, C. Zhang, Q. Feng, Y. Zhang, J. Ning, S. Zhao, H. Zhou, and Y. Hao, *J. Phys. D: Appl. Phys.*, **54**, 243001 (2021).
12. R. M. Gazoni, L. Carroll, J. I. Scott, S. Astley, D. Evans, A. J. Downard, R. J. Reeves, and M. W. Allen, *Physical Review B*, **102**, 035304 (2020).
13. K. Sasaki, M. Higashiwaki, A. Kuramata, T. Masui, and S. Yamakoshi, *Appl. Phys. Express*, **6**, 086502 (2013).
14. F. Ren, J. Yang, C. Fares, and S. Pearton, *MRS Commun.*, **9**, 77 (2019).
15. M. Higashiwaki, K. Sasaki, A. Kuramata, T. Masui, and S. Yamakoshi, *Appl. Phys. Lett.*, **100**, 013504 (2012).
16. T. Oshima, R. Wakabayashi, M. Hattori, A. Hashiguchi, N. Kawano, K. Sasaki, T. Masui, A. Kuramata, S. Yamakoshi, and K. Yoshimatsu, *Jpn. J. Appl. Phys.*, **55**, 1202B1207 (2016).
17. W. A. Callahan, E. Supple, D. Ginley, M. Sanders, B. P. Gorman, R. O'Hayre, and A. Zakutayev, *J. Vac. Sci. Technol. A*, **41**, 043211 (2023).
18. K. Zeng, J. S. Wallace, C. Heimburger, K. Sasaki, A. Kuramata, T. Masui, J. A. Gardella, and U. Singisetti, *IEEE Electron Device Lett.*, **38**, 513 (2017).
19. H. T. Aller, X. Yu, A. Wise, R. S. Howell, A. J. Gellman, A. J. McGaughey, and J. A. Malen, *Nano Lett.*, **19**, 8533 (2019).
20. J.-X. Chen, X.-X. Li, H.-P. Ma, W. Huang, Z.-G. Ji, C. Xia, H.-L. Lu, and D. W. Zhang, *ACS Appl. Mater. Interfaces*, **11**, 32127 (2019).
21. M. Higashiwaki, A. Kuramata, H. Murakami, and Y. Kumagai, *J. Phys. D: Appl. Phys.*, **50**, 333002 (2017).
22. Y. Xiao, X. Li, H. Gong, W. Liu, X. Wu, S. Ding, H. Lu, and J. Ye, *Appl. Surf. Sci.*, **578**, 152047 (2022).
23. Z. Xia, C. Joishi, S. Krishnamoorthy, S. Bajaj, Y. Zhang, M. Brenner, S. Lodha, and S. Rajan, *IEEE Electron Device Lett.*, **39**, 568 (2018).
24. M.-H. Lee and R. L. Peterson, *ACS Appl. Mater. Interfaces*, **12**, 46277 (2020).
25. M.-H. Lee and R. L. Peterson, *APL Mater.*, **7**, 022524 (2019).
26. M.-H. Lee and R. L. Peterson, *J. Mater. Res.*, **36**, 4771 (2021).
27. P. H. Carey, J. Yang, F. Ren, D. C. Hays, S. Pearton, S. Jang, A. Kuramata, and I. I. Kravchenko, *AIP Adv.*, **7** (2017).
28. P. H. Carey, J. Yang, F. Ren, D. C. Hays, S. J. Pearton, A. Kuramata, and I. I. Kravchenko, *J. Vac. Sci. Technol. B*, **35** (2017).
29. J. Yang, S. Ahn, F. Ren, R. Khanna, K. Bevlin, D. Geerpuram, S. Pearton, and A. Kuramata, *Appl. Phys. Lett.*, **110** (2017).
30. J. Yang, F. Ren, R. Khanna, K. Bevlin, D. Geerpuram, L.-C. Tung, J. Lin, H. Jiang, J. Lee, and E. Flitsiyan, *J. Vac. Sci. Technol. B*, **35**, 051201 (2017).
31. D. K. Schroder, *Semiconductor Material and Device Characterization* (John Wiley & Sons, New York) (2015).
32. F. Padovani and R. Stratton, *Solid·State Electron.*, **9**, 695 (1966).
33. J. Swallow, J. Varley, L. Jones, J. Gibbon, L. Piper, V. Dhanak, and T. Veal, *APL Mater.*, **7**, 022528 (2019).
34. C.-C. Chiang, X. Xia, J.-S. Li, F. Ren, and S. Pearton, *Appl. Surf. Sci.*, **631**, 157489 (2023).
35. A. Kyrtsos, M. Matsubara, and E. Bellotti, *Physical Review B*, **95**, 245202 (2017).
36. H. Kim, *SN Appl. Sci.*, **4**, 27 (2021).